Bio-Inspired, Melanin-Like Nanoparticles as a Highly Efficient Contrast Agent for T-1-Weighted Magnetic Resonance Imaging

ARTICLE *in* BIOMACROMOLECULES · AUGUST 2013

Impact Factor: 5.75 · DOI: 10.1021/bm4008138 · Source: PubMed

Article

pubs.acs.org/Biomac

Bio-Inspired, Melanin-Like Nanoparticles as a Highly Efficient Contrast Agent for T_1-Weighted Magnetic Resonance Imaging

Kuk-Youn Ju,[†,‡] Jae Won Lee,[†,§] Geun Ho Im,[§] Sanghee Lee,[∥] Jung Pyo,[‡] Seung Bum Park,[∥] Jung Hee Lee,*[,§] and Jin-Kyu Lee*[,‡]

[‡]Department of Chemistry and [∥]Department of Biophysics and Chemical Biology and Bio-MAX Institute, Seoul National University, Seoul 151-747, Korea

[§]Department of Radiology Samsung Medical Center, Sungkyunkwan University School of Medicine, Seoul 136-710, Korea

Supporting Information

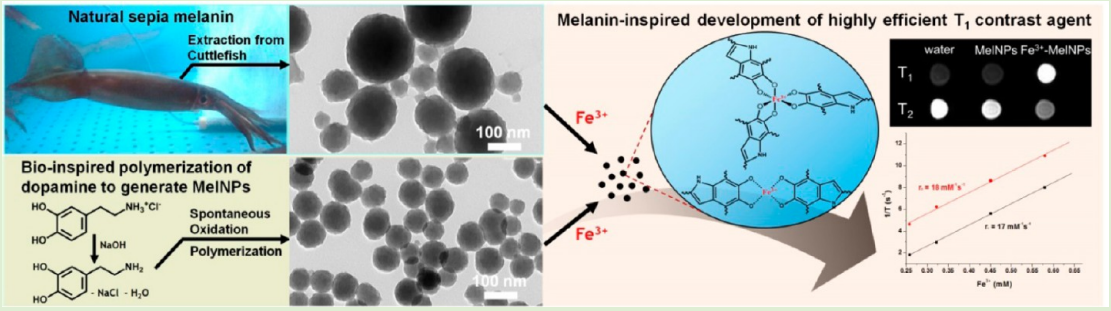

ABSTRACT: The development of nontoxic and biocompatible imaging agents will create new opportunities for potential applications in clinical MRI diagnosis. Synthetic melanin-like nanoparticles (MelNPs), analogous to natural sepia melanin (a major component of the cuttlefish ink), can be used as contrast agent for MRI. MelNPs complexed with paramagnetic Fe^{3+} ions show much higher relaxivity values than existing MRI T_1 contrast agents based on gadolinium (Gd) or manganese (Mn); MelNP values at 3T were r_1 = 17 and r_2 = 18 mM^{-1} s^{-1} (r_2/r_1 value of 1.1). With significant enhancement to MRI contrast, this biomimetic approach using MelNPs functionalized with paramagnetic Fe^{3+} ions and surface-modified with biocompatible poly(ethylene glycol) units, could provide new insight into how melanin-based bioresponsive and therapeutic imaging probes integrate with their various biological functions.

INTRODUCTION

Magnetic resonance imaging (MRI) is one of the most prominent imaging techniques, providing noninvasive anatomical and physiological information with high spatial and temporal resolution.[1] In principle, MRI generates various images of tissue-dependent distributions of water molecules by measuring the magnetic relaxation times of their protons, either in longitudinal T_1 or transversal T_2 mode. The rapid advancement of medical MRI has been accelerated by the development of exogenous contrast agents that effectively decrease the relaxation time of water protons, leading to improved sensitivity and diagnostic accuracy.[2−4] Despite the growing number of clinical MRI scans using contrast agents, low sensitivity, low specificity, and latent toxicity still remain challenging problems while performing an MRI.[5,6] For example, paramagnetic Gd^{3+}, an ion of a nonbiological rare earth metal, has been widely used as a clinical contrast agent because of its high paramagnetic properties resulting from its 7 unpaired f-electrons and its long electronic relaxation time, which efficiently decreases the longitudinal T_1 of water protons. However, Gd^{3+}-based contrast agents must be confined within multidentate organic ligands because of the high toxicity of its free ionic form. In particular, nephrotoxicity issues associated with the Gd ion have been raised recently in clinics, and finding some complementary materials to Gd-based contrast agents is necessary.[7,8] Furthermore, the lack of targeting sites, along with the low blood circulation times of conventional contrast agents, limit their utility as next-generation contrast agents for real-time monitoring of target tissues or cells.

Melanins are pigments found ubiquitously in many parts of living objects. They have attracted much attention because of their involvement in various biological functions, such as photoprotection, photosensitization, free radical quenching, metal ion chelation, and even involvement in nerve systems.[9−11] One of the most important properties of melanins is their ability to strongly chelate metal ions, a vital property in the regulation of metal ions and mitigation of oxidative stress resulting from these redox-active entities in biosystems.[12] Other promising physiochemical properties related with various biological functions have shone a light on melanin as a potential material for a wide scope of applications.[13,14] Interestingly, melanins show significant signal enhancement in

Received: June 4, 2013
Revised: August 27, 2013
Published: August 29, 2013

T_1-weighted MRI owing to their metal ion chelating properties,[15,16] and several attempts have been made to develop melanin-based materials as contrast-enhancing agents.[17] However, their apparently limited dispersibility in aqueous media at physiological pH conditions has led to serious problems in the development of melanin-based contrast-enhancing agents.

Recently, we reported the synthesis of highly water-dispersible, melanin-like nanoparticles (MelNPs), analogous to natural sepia melanin. Because of their stable dispersion properties in water and convenient surface-modification with biofunctional molecules, MelNPs have substantial potential for biomedical applications with target specificity.[18] With the current limitations of MRI contrast agents in mind, we report the complementary material of bioinspired Fe^{3+}-MelNPs with their high biocompatibility and efficient T_1-weighted MRI contrast enhancement, to broaden therapeutic and bioresponsive nanoprobe applications.

EXPERIMENTAL SECTION

Synthesis of Water-Dispersible MelNPs. Water-dispersible MelNPs were prepared according to the procedure in the literature.[18] A total of 180 mg dopamine hydrochloride (Aldrich Chemical) was dissolved in 90 mL of deionized water. Under vigorous stirring, 760 μL of 1 N NaOH solution was added to a dopamine hydrochloride solution at 50 °C. The color of the solution turned to pale yellow as soon as NaOH was added and gradually changed to dark brown. After allowing for reaction for 5 h, MelNPs were retrieved by centrifugation (18000 rpm or 35490 *g*; standard gravity) and washed with deionized water several times. MelNP samples were kept as a dispersed solution after large-sized aggregated materials were removed by low-speed centrifugation (4000 rpm or 2637 *g*).

Size Control of MelNPs. From the standard synthetic conditions described above, the amount of NaOH was changed from 760 to 700 μL, resulting in a size of 318 ± 46 nm (measured by TEM). For a size of 570 ± 100 nm, the volumes of NaOH and water were changed to 670 μL and 45 mL, respectively, from the standard synthetic conditions described above.

Preparation of Sepia Melanin. Ink sacs were obtained from the dissection of Korean cuttlefish. Sepia melanin was extracted by syringe from the freshly dissected ink sac, washed eight times, and centrifuged (18000 rpm) before being redispersed in water to produce a dispersed solution of clean sepia melanin.

Preparation of Fe^{3+}-Sepia Melanin and Fe^{3+}-MelNPs. Preparation of Fe^{3+}-sepia melanin and Fe^{3+}-MelNPs: 100 μL of Fe^{3+} solution (1 mg/mL) was added to 10 mL of sepia melanin solution (1 mg/mL) under vigorous stirring. After 3 h, Fe^{3+}-bound sepia melanin was retrieved by centrifugation (19000 rpm or 39550 *g*). The supernatant was filtered again through a membrane filter (0.45 μm pore size) to measure the concentration difference in Fe^{3+} by ICP-AES to calculate the amount of Fe^{3+} bound to the sepia melanin. The isolated Fe^{3+}-sepia melanin was washed with deionized water several times and diluted to an appropriate concentration for measurements of relaxivity. Various-sized Fe^{3+}-MelNPs (98, 318, and 570 nm) were also prepared and characterized in a similar manner as described above.

Characterization of MelNPs and Fe^{3+}-MelNPs. Infrared spectra were recorded with a JASCO FT-IR-600 Plus. UV/vis spectra were recorded on a SINCO S-3100. ESR spectra were recorded on a JEOL JES-FA200. TEM images were obtained on a Hitachi-7600 electron microscope. The hydrodynamic sizes of prepared MelNPs were measured using an OTSUKA Electronics ELS-8000 electrophoretic light scattering spectrophotometer.

Surface Modification of Fe^{3+}-MelNPs. After 150 mg of methoxy-poly(ethylene glycol)thiol (mPEG-SH, 2 kDa, SunBio, Ahn-Yang, South Korea) was added to 10 mL of Fe^{3+}-MelNP solution (1 mg/mL of water), NH_4OH solution (28 wt %) was added to adjust the pH of the solution to between 9.8 and 10.3. After vigorous stirring for 1 h, surface-modified MelNPs were retrieved by centrifugation (19000 rpm) and washed with deionized water several times using redispersion/centrifugation processes.

***In Vitro* Cytotoxicity Assay (WST-1 Assay).** Cell viability was measured using the WST-1 assay according to the procedure in the manufacturer's manual. Cells were cultured on 96-well plates at a density of 3×10^3 cells/well for 24 h, followed by treatment with compounds in various concentrations. After 24 h of incubation with increasing concentrations, 10 μL of WST-1 solution (2-(4-nitrophenyl)-5-(2-sulfophenyl)-3-[4-(4-sulfophenylazo)-2-sulfophenyl]-2*H*-tetrazolium disodium salt, Daeil Science, Korea) was added to each well, and the plates were incubated for an additional 1 h at 37 °C. The absorbance of each well at 455 nm was measured with a reference at 630 nm by using a Bio-Tek model ELx800TM microplate reader (Bio-Tek Instruments, Winooski, VT), and the absorbance from the MelNPs themselves was compensated for. The percentage of cell viability was calculated using the following formula: % cell viability = (mean absorbance in test wells)/(mean absorbance in control well) × 100. Each experiment was performed in triplicate.

Measuring MRI Relaxation Properties. The Fe^{3+}-MelNPs were prepared in Eppendorf tubes at varying concentrations for imaging. The T_1 and T_2 relaxation times were measured on a 3.0 T clinical MRI scanner (Philips, Achieva ver. 1.2, Philips Medical Systems, Best, The Netherlands), equipped with a gradient amplitude of 80 mT/m and a slew rate of 200 ms/m. Commercially available Gd^{3+}-based contrast agent (DOTAREM, Guerbet, France) was measured in the same manner to compare its contrast-enhancing capability with bioinspired Fe^{3+}-MelNPs. A Look–Locker sequence (TR/TE = 10/1 ms; flip angle = 5°) was used to measure T_1 by acquiring 17 gradient echo images at different inversion delay times. The parameters were as follows: a minimum inversion time of 87 ms; a phase interval of 264 ms; in-plane image resolution = 625 × 625 mm^2; and slice thickness = 500 mm. The images were fitted into a three-parameter function to calculate T_1 values by using a MATLAB program. T_2 measurements were performed using 10 different echo times in a multislice turbo spin echo sequence (TR/TE = 5000/20, 40, 60, 80, 100, 120, 140, 160, 180, 200 ms; in-plane resolution = 200 × 200 mm^2; slice thickness = 500 mm). The images were processed using the Levenberg–Marquardt method to calculate T_2 values using a MATLAB program. We calculated the specific relaxivities (r_1 and r_2) of the nanoparticles from the plots of T_1^{-1} and T_2^{-1} versus concentration of the contrast agent. The signal intensities for each of the ROIs on the T_1 map (60–80 pixels) and the T_2 map (200–300 pixels) were measured for each concentration, which were then used for r_1 and r_2 calculations, respectively. We derived relaxivities based on the molar concentration of iron atoms measured using ICP-AES.

In Vivo MRI Experiment with a Mouse. All in vivo MRI was carried on a 7T/20 micro-MRI System (Bruker-Biospin, Fallanden, Switzerland) equipped with a 20 cm gradient set capable of supplying up to 400 mT/m in a 100 μs rise time. A birdcage coil (72 mm internal diameter) (Bruker-Biospin, Fallanden, Switzerland) was used for excitation, and an actively decoupled phased array coil was used to receive the signal. For in vivo MRI, the animals were anesthetized and set into an MR-compatible cradle. During MRI, the animals were anesthetized with inhalation of 2% isoflurane with oxygen-enriched air through a facemask. The rectal temperature was carefully monitored and maintained at 36 ± 1 °C using a water bath underneath the cradle. The prepared Fe^{3+}-MelNPs (20 μg of MelNPs, 144 μg of Fe measured by ICP-AES per kg of mouse body weight) were intravenously administered through a tail vein of a mouse in the magnet. To investigate the time course distributions of Fe^{3+}-MelNPs in the mouse body, MRI was performed before and 0.5, 1.5, 6, and 24 h after the administrations. High-resolution MelNPs contrast-enhanced multislice MR images were obtained from each mouse abdomen by using a fast spin-echo T_1-weighted MRI sequence (repetition time (TR)/echo time (TE) = 300/7.9 ms; number of experiment (NEX) = 4; echo train length = 2; 100 × 100 μm^2 in plane resolution; slice thickness of 800 μm; and 10 slices), and a fast spin-echo T_2-weighted MRI sequence (repetition time (TR)/echo time (TE) = 3000/60 ms; number of experiment (NEX) = 4; echo train length = 4; 100 × 100 μm^2 in plane resolution; slice thickness of 800 μm; and 10 slices). All

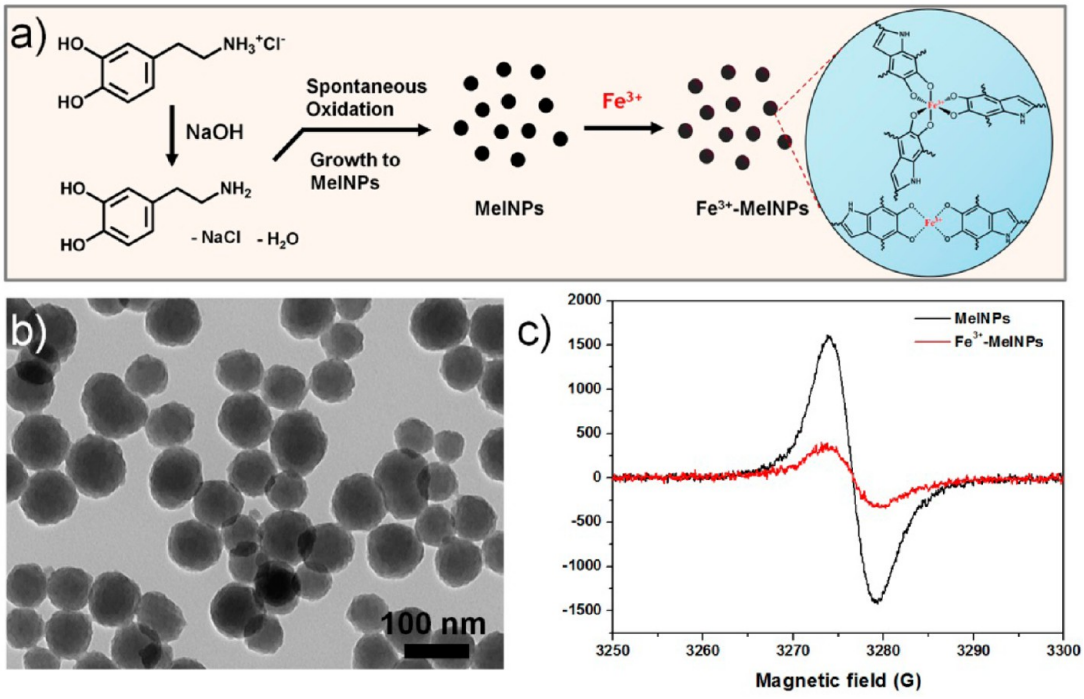

Figure 1. (a) Schematic illustration of the development of efficient T_1-weighted MRI contrast agents using synthetic MelNPs. (b) TEM images of MelNPs and (c) ESR spectra of MelNPs before and after complexation with Fe^{3+} ions.

images were analyzed using Paravasion software (Bruker-Biospin, Fallanden, Switzerland).

RESULTS AND DISCUSSION

MelNPs were prepared with an average size of 98 nm via neutralization of dopamine hydrochloride with NaOH, followed by spontaneous air oxidation of dopamine, as reported in the literature (Figure 1).[18] The high signal intensity of melanin-based material in T_1-weighted MRI is grossly attributed to the complexation of melanin with biologically relevant paramagnetic metal ions, such as Fe^{3+}, Mn^{2+}, and Cu^{2+}.[16] Therefore, the synthetic MelNPs were treated with a Fe^{3+} solution and washed three times, with centrifugation and redispersion in deionized water to prepare Fe^{3+}-bound MelNPs (Fe^{3+}-MelNPs). Electron spin resonance (ESR) signals associated with randomly oriented semiquinone-type free radical species are the very distinctive feature of melanin when compared to other biopolymers; melanin has been used as a molecular probe to determine the presence of paramagnetic or diamagnetic metal ions thorough its comproportionation equilibrium between quinine−quinol units and free radicals.[19−21] Synthetic MelNPs also show single-line ESR spectra associated with their stable free radical, which is a magnetic property similar to that of natural melanin.[18] Therefore, complexation of MelNPs with Fe^{3+} metal ion results in a characteristic decrease of ESR signal, explained by magnetic dipolar interactions between melanin free radicals and paramagnetic metal ions (Figure 1c). The amount of Fe^{3+} bound to the MelNPs was measured using ICP-AES as 7.2 μg of Fe per mg of MelNPs.

The relaxation time of MelNPs and Fe^{3+}-MelNPs were measured using a 3 T clinical MR scanner to investigate the MRI signal−enhancing capability of Fe^{3+}-MelNPs compared to bare MelNPs (Figure 2). As expected, MelNPs without Fe^{3+} ions did not show any appreciable signal enhancement on either T_1- or T_2-weighted MRI, confirming that complexation with paramagnetic Fe^{3+} ions is necessary for MRI signal enhancement. Enhancement of MRI signal induced by complexation with paramagnetic Fe^{3+} ions could be also

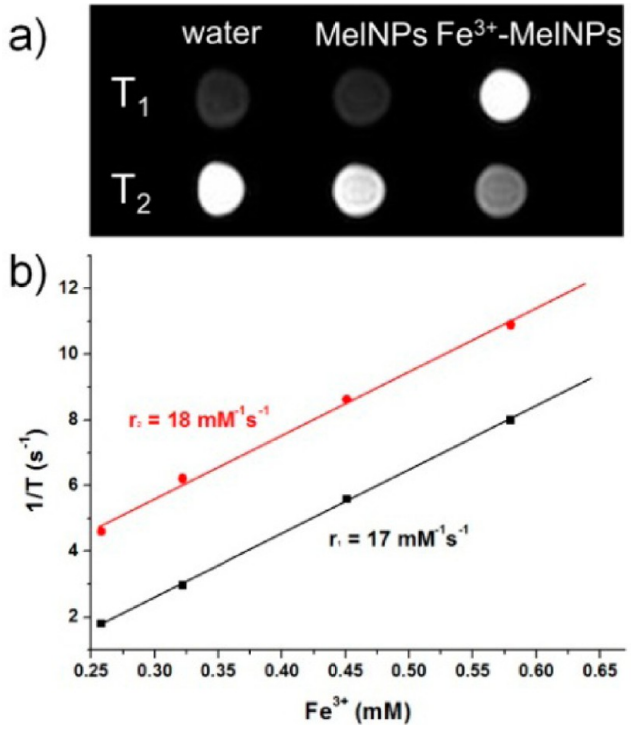

Figure 2. MRI characterizations of bioinspired Fe^{3+}-MelNPs. (a) T_1- and T_2-weighted MRI results from aqueous suspensions of Fe^{3+}-MelNPs with respect to bare MelNPs and deionized water (the concentration of each sample was adjusted to 4 mg/mL). (b) Plots of $1/T_1$ and $1/T_2$ vs Fe^{3+} concentration for Fe^{3+}-MelNPs.

dx.doi.org/10.1021/bm4008138 | Biomacromolecules 2013, 14, 3491−3497

Table 1. Relaxivity Data for Representative T_1 Contrast Agents

contrast agent	diameter (nm)	r_1 (mM^{-1} s^{-1})	r_2 ($mM^{-1}s^{-1}$)	r_2/r_1	B_0 (T)	ref
Gd-DOTA[a]	single molecule	7.1	6.6	1.06	3	present study
Fe_2O_3	2.2	4.7	17.5	3.6	3	32
MnO	7	0.3	1.7	4.7	3	33
HMON	20	1.4	7.7	5.5	3	34
Fe^{3+}-MelNP	98	17	18	1.1	3	present study

[a]Gd-DOTA; commercially available Gd complex of 1,4,7,10-tetraazacyclododecane-1,4,7,10-tetraacetic acid, data shown in Figure S3

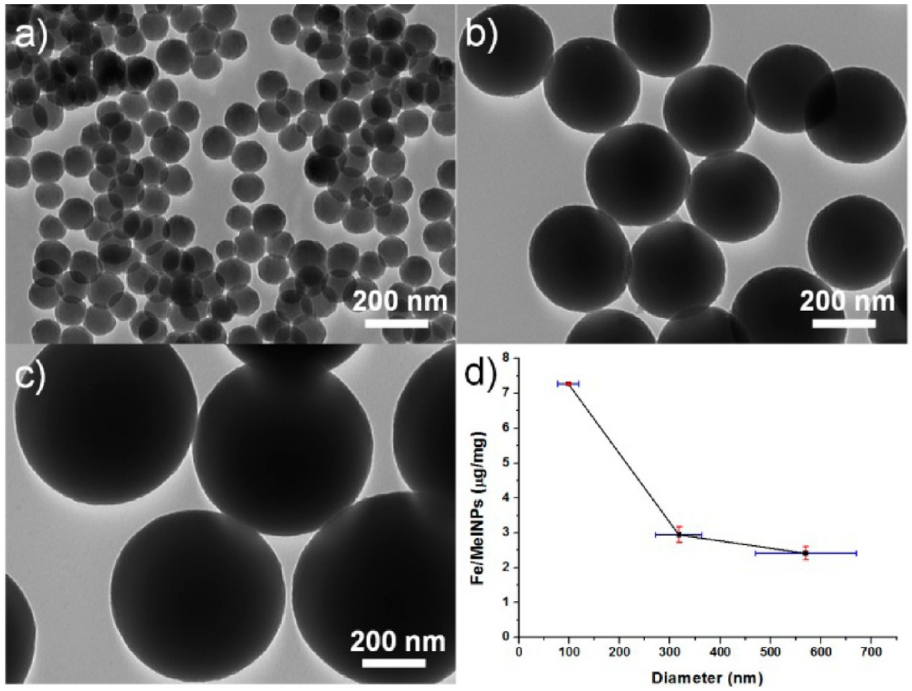

Figure 3. Amount of Fe^{3+} on Fe^{3+}-MelNPs showed size-dependent Fe^{3+} binding capacity in the same complexation conditions. (a–c) TEM images of differently sized MelNPs. (d) Size-dependent Fe^{3+} binding capability of MelNPs.

confirmed in the case of sepia melanin, a well-known natural melanin model (see Supporting Information, Figure S1). By measuring the variation in relaxation times of samples at different concentrations, the relaxation rates (reciprocal values of relaxation times) were plotted against the amount of bound Fe^{3+} ions ($1/T$ vs $[Fe^{3+}]$) and relaxivity values (r_1 and r_2; the slopes of each plot, mM^{-1} s^{-1}) were determined to be $r_1 = 17$ and $r_2 = 18$ for Fe^{3+}-MelNPs (Figure 2b). The relaxivity values are much higher than those of clinically–used Gd^{3+}-based contrast agents (Table 1). More interestingly, the r_2/r_1 value of MelNP after Fe^{3+} complexation was 1.1, suggesting their efficacy as a T_1 contrast agent, as agents with low r_2/r_1 values are commonly suitable for T_1-weighted contrast enhancement. From the contrast-enhancing effect of Fe^{3+}-MelNPs inspired by natural melanin, it is possible that MelNPs have physicochemical parameters similar to that of natural melanin, which contribute to the shorter relaxation times, such as complex structure and dynamics in solution. Brown-black eumelanin, the predominant type of natural melanin, is composed of several basic monomers, such as 5,6-dihydroxyindole (DHI), 5,6-dihydroxyindole-2 carboxylic acid (DHICA), pyrrole, and DOPA, with various metal binding sites.[17,22–24] In the case of binding Fe^{3+}, the *o*-dihydroxyl group of the catechol unit has proven much more important for the Fe^{3+} ion to form 4–6 coordinate high-spin complexes with distorted octahedral or rhombic symmetry (Figure 1).[25] In the same manner, catechol units of MelNPs could play a central role in the Fe^{3+} complex structure because MelNPs are generated by the oxidative polymerization of dopamine. The exceptionally high contrast enhancement capability of Fe^{3+}-MelNPs on T_1-weighted MRI may be attributed to its characteristic *o*-dihydroxyl group of catechol that enables water molecules to bond to oxygen atoms of catecholate Fe^{3+} complex in a so-called second-sphere hydrogen bonding manner, which is accompanied by a further enhancement advantage in r_1 relaxivity. According to the Solomon–Bloembergen–Morgan (SBM) theory predicting the efficiency of MRI contrast agents, longitudinal relaxivity is divided into two parts: inner sphere relaxation, which is influenced by directly coordinated water molecules, and outer sphere relaxation, which arises from interaction of the complex with water molecules in the second and outer spheres.[3] Although the predominant effect of inner sphere relaxation is on r_1 relaxivity, experimental studies on catecholate–Fe^{3+} complexes have shown that the contribution from interactions between second-sphere water molecules and oxygen atoms in these complexes is important for its unusually high enhancing capabilities.[26,27] In addition, the nanoparticulate character of melanin is expected to yields additional benefits for relaxivity enhancement, because confinement of the paramagnetic complex within a nanocarrier generally results in an enhancement of r_1 relaxivity, which is primarily explained by the restricted rotational mobility of the complex.[28,29]

dx.doi.org/10.1021/bm4008138 | *Biomacromolecules* 2013, 14, 3491–3497

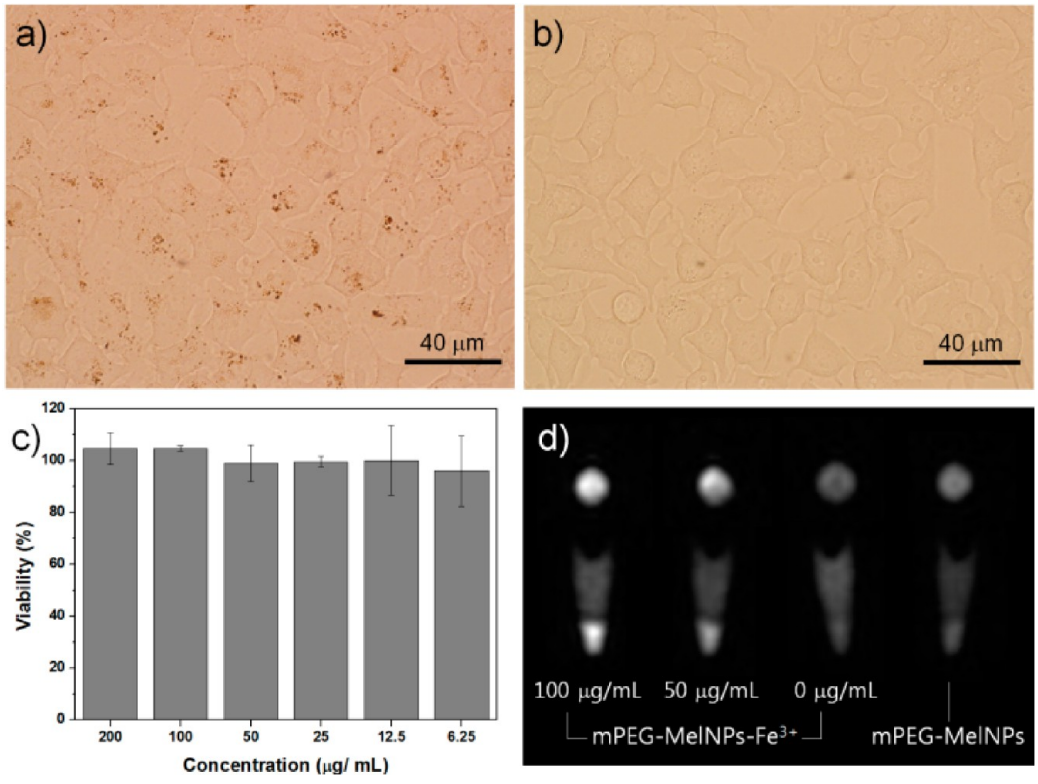

Figure 4. (a) Optical microscope image of HeLa cells incubated with PEGylated Fe^{3+}-MelNPs (200 g/mL) for 24 h compared to (b) HeLa cells as a control, (c) WST-1 cytotoxicity assay for HeLa cells incubated with various concentrations of PEGylated Fe^{3+}-MelNPs, and (d) T_1-weighted MR images of HeLa cells incubated at different conditions.

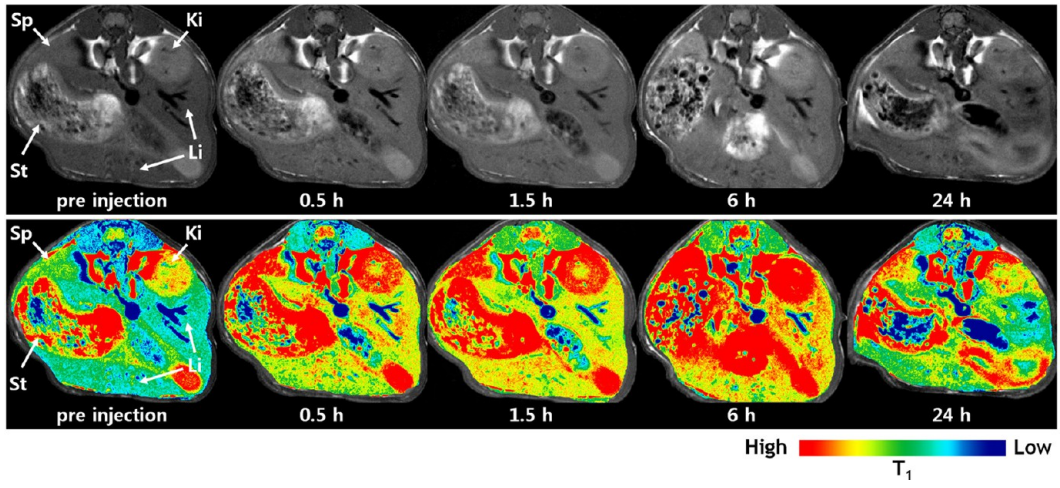

Figure 5. T_1-weighted MR and color-mapped images of a mouse at different time intervals after intravascular injection of PEGylated Fe^{3+}-MelNPs. Arrows indicate the spleen (Sp), kidney (Ki), liver (Li), and stomach (St).

To further investigate the contrast enhancement effect of MelNPs, the Fe^{3+} binding capability of differently sized MelNPs was examined. The paramagnetic complex is responsible for shortening the T_1 relaxation time, therefore, the site of the Fe^{3+} complex on MelNPs predominates for contrast enhancement. Differently sized MelNPs exhibited size-dependent Fe^{3+} binding properties under the same conditions (Figure 3). This can be explained by the fact that the Fe^{3+} binding sites on MelNPs are closely correlated with the surface-to-volume ratio of MelNPs. Based on the size-dependent Fe^{3+} binding properties of MelNPs, Fe^{3+} complexes could shorten the T_1 relaxation time, primarily on their surface.

The development of suitable methods for surface modification of nanoparticles plays an important role in providing a wide range of functionality for biomedical applications. Melanin-like nanoparticles provide an immobilization site for amine- or thiol-functionalized molecules, possibly via a Schiff base or Michael addition reaction,[30] and consequently, their surface chemistry makes them a promising nanoplatform for a variety of biomedical purposes.[18] By using Fe^{3+}-MelNPs' surface chemistry, the surface of these particles can be functionalized with thiol-terminated methoxy-poly(ethylene glycol) (mPEG-SH), which is known to render nanoparticles stable against biofouling and aggregation for extended periods

dx.doi.org/10.1021/bm4008138 | Biomacromolecules 2013, 14, 3491−3497

of time under physiological conditions. Even though the PEGylation of Fe^{3+}-MelNPs slightly increases their relaxivity, possibly through a change in the dynamics of water molecules toward the paramagnetic complex on MelNPs, PEGylated Fe^{3+}-MelNPs did not show significant changes in relaxivity, confirming that the binding ability of Fe^{3+} on MelNPs was not influenced by the surface modification of MelNPs with mPEG-SH (see Supporting Information, Figure S2).

Although the cell viability of PEGylated MelNPs had already been confirmed,[18] the cytotoxicity of PEGylated Fe^{3+}-MelNPs was further evaluated with a WST-1(4-[3-(4-iodophenyl)-2-(4-nitrophenyl)-2*H*-5-tetrazolio]-1,3-benzene-disulfonate) assay in HeLa cells (human cervical carcinoma cells; Figure 4c). PEGylated Fe^{3+}-MelNPs did not show any acute cytotoxicity or morphological changes after incubation with PEGylated Fe^{3+}-MelNPs at levels up to 200 μg/mL within 24 h, promising nontoxic applications to living systems. As expected, optical microscope images of HeLa cells incubated with PEGylated Fe^{3+}-MelNPs showed possible internalization of MelNP into HeLa cells through endocytosis (Figure 4a,b). T_1-weighted MR images of HeLa cell pellets after 12 h incubation with different concentrations of PEGylated Fe^{3+}-MelNPs exhibited T_1 signal enhancement in a concentration-dependent manner (Figure 4d).

On the basis of their low cytotoxicity, the actual efficacy of PEGylated Fe^{3+}-MelNPs for in vivo MRI imaging was investigated. For in vivo MR imaging, PEGylated Fe^{3+}-MelNPs were administered to a mouse through the tail vein. After injection, positive signal enhancement of T_1-weighted MRI images in the spleen and the liver were observed within 0.5 and 1.5 h, respectively, perhaps because of the selective accumulation of PEGylated Fe^{3+}-MelNPs in the cells of the reticuloendotherial system (RES; Figure 5). After 6 h, the liver seemed to return to a similar contrast to that before administration, but apparently high signal enhancement in the spleen persisted. From the viewpoint of the accumulation pathway through the RES and the long residual times, these results are very similar to those reported on inorganic nanoparticles for MRI contrast agents.[31] More interestingly, after 24 h, all organs seemed to return to normal contrast in T_1-weighted MRI images, indicating the degradation, clearance of Fe^{3+}-MelNPs, and detachment of Fe^{3+} from MelNPs. More detailed studies are needed to understand the fate of Fe^{3+}-MelNPs compared to other artificial inorganic nanoparticles.

CONCLUSIONS

In conclusion, we introduced a highly efficient and optimized T_1 MRI contrast agent by using synthetic MelNPs, inspired by the novel MRI signal-enhancing capability of natural melanin. Especially in light of recent claims about the nephrotoxicity of Gd^{3+}-based contrast agents, which has emphasized the importance and high demand for the development of nontoxic and efficient T_1-MRI contrast agents, the bioinspired T_1-MRI contrast-enhancing nanoprobe discussed herein provides not only a new platform with promising applications in diagnostic radiology and nanoprobe imaging but also an insight into the development of highly efficient and biocompatible melanin-based T_1 MRI contrast agents.

ASSOCIATED CONTENT

Supporting Information

Quantitative analysis of Fe bound to MelNPs and sepia, characterization of surface modification of Fe^{3+}-MelNP, and relaxivity data for commercially available Gd-DOTA. This material is available free of charge via the Internet at http://pubs.acs.org.

AUTHOR INFORMATION

Corresponding Author

*E-mail: hijunghee@skku.edu; jinklee@snu.ac.kr.

Author Contributions

†These authors contributed equally (K.-Y.J., J.W.L.).

Notes

The authors declare no competing financial interest.

ACKNOWLEDGMENTS

This research was partially supported by the Basic Science Research Program through the National Research Foundation (NRF) grant funded by the Korean government (2010-0027955) and by the Seoul National University Brain Fusion Program Research Grant. K.-Y.J., J.P., and S.L. gratefully acknowledge the BK21 fellowship.

REFERENCES

(1) Lauffer, R. B. *Chem. Rev.* **1987**, *87*, 901−927.
(2) Caravan, P.; Ellison, J. J.; McMurry, T. J.; Lauffer, R. B. *Chem. Rev.* **1999**, *99*, 2293−2352.
(3) Hermann, P.; Kotek, J.; Kubicek, V.; Lukes, I. *Dalton Trans.* **2008**, 3027−3047.
(4) Caravan, P. *Chem. Soc. Rev.* **2006**, *35*, 512−523.
(5) Raymond, K. N.; Pierre, V. C. *Bioconjugate Chem.* **2005**, *16*, 3−8.
(6) Aime, S.; Castelli, D. D.; Crich, S. G.; Gianolio, E.; Terreno, E. *Acc. Chem. Res.* **2009**, *42*, 822−831.
(7) Ledneva, E.; Karie, S.; Launay-Vacher, V.; Janus, N.; Deray, G. *Radiology* **2009**, *250*, 618−628.
(8) Fujisaki, K.; Ono-Fujisaki, A.; Kura-Nakamura, N.; Komune, N.; Hirakawa, N.; Tsuruya, K.; Komune, S.; Iida, M. *Clin. Nephrol.* **2011**, *75*, 251−254.
(9) Hill, H. Z. *BioEssays* **1992**, *14*, 49−56.
(10) Meredith, P.; Sarna, T. *Pigm. Cell Res.* **2006**, *19*, 572−594.
(11) Meredith, P.; Powell, B. J.; Riesz, J.; Nighswander-Rempel, S. P.; Pederson, M. R.; Moore, E. G. *Soft Matter* **2006**, *2*, 37−44.
(12) Hong, L.; Simon, J. D. *J. Phys. Chem. B* **2007**, *111*, 7938−7947.
(13) Meredith, P.; Bettinger, C. J.; Irimia-Vladu, M.; Mostert, A. B.; Schwenn, P. E. *Rep. Prog. Phys.* **2013**, *76*, 034501.
(14) Bettinger, C. J.; Bruggeman, J. P.; Misra, A.; Borenstein, J. T.; Langer, R. *Biomaterials* **2009**, *30*, 3050−3057.
(15) Gomori, J. M.; Grossman, R. I.; Shields, J. A.; Augsburger, J. J.; Joseph, P. M.; Desimeone, D. *Radiology* **1986**, *158*, 443−445.
(16) Enochs, W. S.; Petherick, P.; Bogdanova, A.; Mohr, U.; Weissleder, R. *Radiology* **1997**, *204*, 417−423.
(17) Hung, Y. C.; Sava, V. M.; Juang, C. L.; Yeh, T. C.; Shen, W. C.; Huang, G. W. S. *J. Ethnopharmacol.* **2002**, *79*, 75−79.
(18) Ju, K. Y.; Lee, Y.; Lee, S.; Park, S. B.; Lee, J. K. *Biomacromolecules* **2011**, *12*, 625−632.
(19) Sarna, T.; Hyde, J. S.; Swartz, H. M. *Science* **1976**, *192*, 1132−1134.
(20) Felix, C. C.; Hyde, J. S.; Sarna, T.; Sealy, R. C. *J. Am. Chem. Soc.* **1978**, *100*, 3922−3926.
(21) Commoner, b.; Townsend, J.; Pake, G. E. *Nature* **1954**, *174*, 689−691.
(22) Borovansky, J.; Elleder, M. *Pigm. Cell Res.* **2003**, *16*, 280−286.
(23) Napolitano, A.; Pezzella, A.; Vincensi, M. R.; Prota, G. *Tetrahedron* **1995**, *51*, 5913−5920.
(24) Watt, A. A. R.; Bothma, J. P.; Meredith, P. *Soft Matter* **2009**, *5*, 3754−3760.
(25) Nordlund, J. J. *The Pigmentary System*; Blackwell Publishing, Inc.: Malden, 2006; Vol. 2, p 345.

(26) Aime, S.; Botta, M.; Ermondi, G.; Fasano, M.; Terreno, E. *Magn. Reson. Imaging* **1992**, *10*, 849−854.
(27) Davies, J. A.; Dutremez, S. G.; Hockensmith, C. M.; Keck, R.; Richardson, N.; Selman, S.; Smith, D. A.; Ulmer, C. W.; Wheatley, L. S.; Zeiss, J. *Acad. Radiol.* **1996**, *3*, 936−945.
(28) Xu, H.; Regino, C. A.; Bernardo, M.; Koyama, Y.; Kobayashi, H.; Choyke, P. L.; Brechbiel, M. W. *J. Med. Chem.* **2007**, *50*, 3185−3193.
(29) Ananta, J. S.; Godin, B.; Sethi, R.; Moriggi, L.; Liu, X. W.; Serda, R. E.; Krishnamurthy, R.; Muthupillai, R.; Bolskar, R. D.; Helm, L.; Ferrari, M.; Wilson, L. J.; Decuzzi, P. *Nat. Nanotechnol.* **2010**, *5*, 815−821.
(30) Lee, H.; Dellatore, S. M.; Miller, W. M.; Messersmith, P. B. *Science* **2007**, *318*, 426−430.
(31) Na, H. B.; Song, I. C.; Hyeon, T. *Adv. Mater.* **2009**, *21*, 2133−2148.
(32) Kim, B. H.; Lee, N.; Kim, H.; An, K.; Park, Y. I.; Choi, Y.; Shin, K.; Lee, Y.; Kwon, S. G.; Na, H. B.; Park, J. G.; Ahn, T. Y.; Kim, Y. W.; Moon, W. K.; Choi, S. H.; Hyeon, T. *J. Am. Chem. Soc.* **2011**, *133*, 12624−12631.
(33) Na, H. B.; Lee, J. H.; An, K.; Park, Y. I.; Park, M.; Lee, I. S.; Nam, D. H.; Kim, S. T.; Kim, S. H.; Kim, S. W.; Lim, K. H.; Kim, K. S.; Kim, S. O.; Hyeon, T. *Angew. Chem., Int. Ed.* **2007**, *46*, 5397−5401.
(34) Shin, J. M.; Anisur, R. M.; Ko, M. K.; Im, G. H.; Lee, J. H.; Lee, I. S. *Angew. Chem., Int. Ed.* **2009**, *48*, 321−324.